# Method Based on Continuous Artificial Dry and Humid UV Treatments to Reduce the Luminescence Background in the Raman Spectra of Plastics

L. Dewyspelaere, L. Belec, I. Martin, V. Lenoble, A. Ruediger, A. Merlen

*Journal of Raman Spectroscopy*

WILEY

Journal of RAMAN SPECTROSCOPY

RESEARCH ARTICLE OPEN ACCESS

# Method Based on Continuous Artificial Dry and Humid UV Treatments to Reduce the Luminescence Background in the Raman Spectra of Plastics

L. Dewyspelaere[1] | L. Belec[1] | I. Martin[1] | V. Lenoble[2] | A. Ruediger[3] | A. Merlen[1]

[1]MAPIEM, Université de Toulon, Toulon, France | [2]MIO, Université de Toulon, Aix Marseille Univ., CNRS, IRD, Toulon, France | [3]Nanoélectronique-Nanophotonique, Institut National de la Recherche Scientifique – Centre Energie, Matériaux et Télécommunications (INRS-EMT), Varennes, Québec, Canada

**Correspondence:** A. Merlen (merlen@univ-tln.fr)

**Received:** 17 October 2025 | **Revised:** 27 February 2026 | **Accepted:** 2 March 2026

**Keywords:** biofilm | luminescence background | pigments | plastic pollution | Raman spectroscopy | UV treatment

## ABSTRACT

The applicability of short continuous artificial UV treatments has been studied to reduce the luminescence background in Raman spectra of plastics. Our method applies to two groups of polyethylene plastics, in which luminescence arises either from pigments or from surface contaminations such as biofilm or from a combination of both. Increasing the duration of continuous UV exposure resulted in decreased luminescence due to photobleaching. The evolution of surface morphology and chemical composition was monitored using optical spectromicroscopy. With progressive photobleaching, the signal-to-noise ratio of first-order Raman signatures improved, facilitating spectral analysis. In particular, we achieved a correlation rate exceeding 90% in the identification of polymers and their additives after treatment, which is mainly limited by the availability of reference databases. While the procedure allows for the rapid and non-destructive identification of polymeric species, it induces only minor chemical modifications at the surface, including the oxidation of functional groups.

## 1 | Introduction

Since the middle of the twentieth century, a fast increase of the world plastics production is observed [1]. In 2023, the global plastic production was estimated at 413.8 million metric tons (Mt) [1, 2]. Between 1950 and 2015, 6300 Mt of plastics were manufactured: 12.7% and 9.5% were incinerated and recycled, respectively [3]. The remainder (77.8%) was discharged and accumulated in the environment [3]. None of the commonly used plastics are biodegradable, which generates plastic waste in all environmental compartments [4–6]. The omnipresence of plastics in the atmospheric, marine, and terrestrial environments is well-documented [7, 8]. In the long term, this waste is subject to fragmentation into micro- and nano-plastics under the effect of external conditions (solar radiation, oxidation, mechanical abrasion, etc.) [9–11]. A decrease in the size of particles increases the risk to release additives and of ingestion by terrestrial and marine animals [12, 13].

In order to visualize the nature of plastic pollution, it is necessary to have access to reliable chemical identification methods [14]. Infrared and Raman spectroscopy are widely used and recognized techniques in the scientific community [5, 15, 16] thanks to their non-destructive characteristics without specific preparation and small sample quantities [17–20]. While infrared absorption spectroscopy generally provides a substantially higher cross section than Raman spectroscopy, the latter becomes comparable and even stronger in the case of resonant-Raman conditions, i.e., when the incident radiation is absorbed, which is typically the case for additives. Moreover, Raman spectroscopy provides a superior spatial resolution (typically better than 1 μm) to infrared spectroscopy (few microns) [20–22]. The

ability to detect small quantities of constituents, combined with high sensitivity to many additives such as pigments, has established Raman spectroscopy as a relevant method for microplastics identification [23, 24].

A key limitation for the use of Raman spectroscopy is the presence of photoluminescence [17, 20, 25]. Occurring in the same spectral range as Raman scattering and displaying a cross-section that exceeds that of the Raman effect by several orders of magnitude, it leads to broad and intense bands masking (partially or completely) the Raman signature [26]. When photoluminescence is too intense, chemical identification becomes impossible [27]. More specifically, the intensity of Raman bands should exceed the statistical noise of the luminescence signature. The latter may be caused by impurities, defaults, absorption of the molecule itself, or its interaction with other components [28, 29].

Photoluminescence in polymers originates either from the backbone, which generally requires UV excitation, additives with absorption in the visible range, and adsorbates including biofilms and chemisorbates. In our pristine samples, at an excitation wavelength of 632.8 nm, which corresponds to 1.96 eV, photoluminescence is associated with additives (pigments) or defaults to produce a luminescent background [1, 5, 23]. The interference between pigment-associated photoluminescence and Raman signature is strongest, when the laser excitation wavelength is close to the main emission of the dye, and therefore overlaps with the relatively weak Raman shift [19, 30]. For our aged samples, additional contributions to photoluminescence are generated by surface contaminations, in particular when a biofilm is formed (in the case of plastics in the sea, for example) [31–33]. Encountered during natural aging, biofilm development on the substrate surface is known to involve strong luminescence, preventing Raman identification [18]. The removal of the biofilm is complex and generally involves chemical treatments. Consequently, using Raman spectroscopy in the field of plastic pollution requires preliminary measures to minimize luminescence arising from those different sources.

Various studies aimed at the reduction of the luminescence background by pre-treatment (photobleaching, oxidative treatments), wavelength modifications or time-gated Raman spectroscopy [33]. Photobleaching involves successive irradiations of the sample to degrade the luminescent compound [23]. Photobleaching is usually performed with the Raman laser itself. Reports have shown a decrease in luminescence associated with an increase in the signal-to-noise ratio for Raman spectroscopy [34] to the point that an identification of the pigments or polymer becomes possible [1]. Dongkwon et al. [1] noted an accelerated decrease in luminescence when the laser power is increased or when pigment concentration or particle size are decreased, but only the laser power is experimentally accessible for the case of environmental investigations. Laser-induced photobleaching is efficient as it occurs at the very spot of observation in a confocal Raman-spectroscopy setup. Already for moderate laser powers of 1 mW and a diffraction-limited focal area in the range of 1 square micron, the intensity is in the range of 1 $GW/m^2$. The obvious risk upon absorption is that the treatment will not be limited to photobleaching but might induce irreversible oxidation if not pyrolysis of the sample [17]. In particular, in the case of biofilms, the confocal depth is insufficient to photobleach all possibly interfering fluorophores, so that our approach is directed towards an external treatment. Moreover, Macdonald et al. [17] observed possible physical or chemical modifications of certain sample components during prolonged exposure to intense laser radiation (25 mW on a diffraction limited spot) at 785 nm.

Explicit oxidative treatments have been proposed as a way to overcome the luminescence background. Liu et al. [35] demonstrated the effectiveness of Fenton's agent ($Fe^{3+}$, $Fe^{2+}$, $Fe_3O_4$, and $K_2Fe_40_7$) to generate hydroxyl radicals (in presence of $H_2O_2$) to suppress the luminescent agent. For all colored plastics, they obtained positive identifications with match scores above 70%. A discoloration of the samples was observed with a progressive disappearance of the plastic additive peaks on the Raman spectra after treatment [35].

Another strategy is the use of lower excitation energies or higher wavelengths to avoid electronic transition [25, 36–39]. The increase of wavelength leads to a decrease in the Raman scattering cross section (in relation with the $1/\lambda$ [4] Raman cross section) [27, 40]. To compensate, substantially longer acquisition times are required [18]. This method does however not suppress luminescence in all cases. Additionally, changing the excitation wavelength to the point that conditions for resonant Raman excitation are no longer met may result in a loss of information in the analyzed spectral range [36].

Finally, with the recent technological advances in detectors, time-gated Raman spectroscopy has become increasingly popular [41–43]. Based on the use of short pulse lasers and time-gated detectors, it exploits the difference in lifetimes between Raman scattering (picoseconds or shorter-instrumentally limited) and luminescence emission (nanoseconds) [44, 45]. While the Raman signal is collected, the luminescence is discarded during the detector's idle time [27]. Kotula et al. [18] observed a decrease of luminescence background with time-gated Raman spectroscopy on plastics leading to possible identification of additives and polymers. They also demonstrated an improvement in efficiency as the pulsed laser emission time decreases [18]. Actually, its use is limited by the requirement of a pulsed laser and specific detector to perform the measurements.

The present study presents preliminary observations of luminescence reduction obtained on samples aged under different environmental conditions. Conventional photobleaching with the Raman laser was performed to reduce the luminescence, but this approach was insufficient to observe the polymer's Raman modes or resulted in irreversible transformation of the sample into amorphous carbon depending on the laser wavelength and intensity. Unlike conventional photobleaching, which only reduces luminescence where the laser interacts with the sample, the process implemented here uses external illumination to expose all surfaces. Our treatment provides sufficient efficiency to photobleach fluorophores and, compared to conventional photobleaching, bears a reduced risk of sample destruction. The originality of this article lies in the optimization of the treatment conditions (exposure wavelength, irradiance, humidity) to maximize treatment efficiency. Our treatment provides a compromise between sufficiently good

**TABLE 1** | Summary of the five types of UV treatments used to reduce luminescence.

| Aging chambers | Types of treatments | Exposure period | Lamp type | Irradiance ($W\,m^{-2}$) | Temperature (°C) | Effect of … |
|---|---|---|---|---|---|---|
| QUV/se models (Q-LAB) | **UV-076** | 24 h UV | UVA–340 nm | 0.76 | 45 | … irradiance |
| | **UV-083** | 24 h UV | UVA–340 nm | 0.83 | 45 | |
| | **UV-night** | 8 h UV<br>4 h night phase | UVA–340 nm<br>x | 0.76<br>x | 60<br>50 | … humidity phase (temperature) |
| | **Humid UV** | 8 h UV<br>4 h condensation phase | UVA–340 nm<br>x | 0.76<br>x | 60<br>50 | |
| Novascan UV ozone cleaners | **UV ozone** | 15, 30, 60, 120, 180, 240, 300, 420, 540, 660 min | 254 nm<br>185 nm | x | x | … wavelength |

photobleaching to reach the detection threshold of Raman spectroscopy and sufficiently low absorption to preserve the integrity of the sample. Particular attention is paid to the impact of our treatments on the composition and surface morphology of the samples, while the study also includes Raman monitoring of biofilm-coatings during treatments. The treatments are effective, as they allow for a straightforward identification of the host matrix and are easy to implement, cost- and time-efficient without chemical treatment, and still only require a single excitation wavelength.

## 2 | Materials and Methods

### 2.1 | Samples

To demonstrate the effectiveness of the different treatments on the luminescence, two batches of commercial high-density polyethylene caps were studied. We also discriminate against the origin of the luminescence, i.e., whether it is caused by pigments (first group) or to surface contaminants (second group). Due to industrial secret, their exact composition was unknown. Other color samples, including red, were collected but discarded because their Raman spectrum did not show luminescence.

The first batch consists of two samples, green and blue bottle caps, in order to ensure the applicability of our approach to different pigments. The second batch contains white bottle caps (non-luminescent in the visible) covered by a biofilm layer to control the effectiveness of the treatments on bioluminescence. These caps were immersed in seawater in the Bay of Toulon for 3 weeks, the time required for the microorganisms to colonize the surface samples. The presence of the biofilm was confirmed by optical microscopy observations, see Figure 5. All those samples are typical pollutants identified in the sea environment.

### 2.2 | UV Treatment

Five treatments with different UV conditions (irradiance, presence of humidity, and wavelength) have been set up to observe their effects on the photoluminescence phenomenon (Table 1). The UV radiation is usually classified as UV-A (400–315 nm), UV-B (315–280 nm), and UV-C (280–100 nm). To achieve different wavelengths, two UV aging chambers have been used. The QUV/se model from Q-LAB is equipped with lamps with an emission wavelength of 340 nm (UVA), a humidity-controlled chamber, and a device for programming exposure cycles. UVA is preferred for aging in QUV chambers since it is more representative of natural sunlight. On the other hand, a UV ozone cleaner with two emission wavelengths of 254 nm (UVC) and 185 nm (UVC) was also used to excite molecules and produce ozone (no ozone was intentionally introduced in the chamber), respectively. The differences in emission wavelength and the presence or absence of humidity are the factors that differentiate the two aging chambers. UVC was used for surface treatment equipment, as it is more aggressive [46]. The sample-to-lamp distance was similar for the two aging chambers. The use of external illumination offers the advantage of processing several samples simultaneously.

The QUV/se models have been employed for the first four treatments. The exposure times were set to 1, 2, and 3 days. First, an irradiance of $0.76\,W\,m^{-2}$ at 45 °C has been performed and labeled "UV-076." Second, to determine the impact of irradiance, the temperature was kept constant and the irradiance was increased to $0.83\,W\,m^{-2}$ ("UV-083" treatment). Third, an intermediate treatment "UV-night" was realized to add a second phase in the treatment. This "UV-night" treatment was used as a reference for the fourth treatment. The cycle was composed by UV radiation phase during 8 h and 4 h of "night phase" (UV lamp was off). For the UV radiation, an irradiance of $0.76\,W\,m^{-2}$ with a temperature of 60 °C was fixed. During the "night phase," the temperature was kept at 50 °C. Fourth, the treatment "humid UV" was implemented to study the influence of humidity cycle. It was carried out with a succession of 8 h of UV irradiation ($0.76\,W\,m^{-2}$, 60 °C) and 4 h of humidity. The humidity was produced by evaporation of water in the chamber and was constantly above 100%. The temperature during the humidity phases was retained at 50 °C by the presence of hot vapor in the test chamber.

To observe the effect of the irradiation wavelength, a UV ozone cleaner was used for the fifth treatments. The choice of this

equipment was motivated by its convenient accessibility in the laboratory and its regular use for cleaning surfaces. Samples that exhibited luminescence related to pigments or surface contamination were aged for successive periods of 15, 30, 60, 120, 180, 240, 300, 420, 540, and 660 min.

## 2.3 | Monitoring Luminescence and Simultaneously Controlling Surface Modifications

### 2.3.1 | Experimental Procedure

Raman and infrared spectroscopy were used to monitor the decrease in luminescence and to understand the chemical changes induced by the UV treatments, respectively. Surface alteration was controlled by optical microscopy.

In this study, pristine samples containing different pigments and immersed samples covered with biofilm (surface-related luminescence) were analyzed. For pristine samples, a Raman and infrared spectrum each were acquired at three different positions. For immersed samples, the Raman spectrum was obtained on a reproducible, single location. This choice was guided by the biofilm's heterogeneous development at the microscopic scale. Moreover, infrared measurements were impossible due to the irreversible interaction of the ATR crystal and the biofilm.

For all Raman acquisition, two spectral ranges between 700–1800 $cm^{-1}$ and 2700–300 $cm^{-1}$ were acquired. The luminescence was quantified centered at 1300 $cm^{-1}$ (between 700 and 1800 $cm^{-1}$) corresponding to its highest intensity. The ordinate of the point was defined as the maximum intensity and called "I max." A decrease of the luminescence was reflected by a decrease of the "I max" upon treatment. The second spectral range, around 3000 $cm^{-1}$ (between 2700 and 3200 $cm^{-1}$) was used to evaluate the match score (from a polymer database [47] included on the Wire software) with the correlation methods [48–50]. To compare with the polymer library, the spectra were first treated with a subtract baseline correction. For infrared data, preprocessing included the baseline subtraction, and normalization was performed with Spectragryph [51] software.

### 2.3.2 | Spectroscopy to Evaluate Luminescence

Samples were analyzed with a Raman microspectrometer (Renishaw) coupled to an optical microscope (Leica) equipped with a camera. A He-Ne laser (633 nm, ~13 mW) was used as the source of excitation. The laser beam was focused on the samples' surface by a 20× objective lens (0.4 numerical aperture), and the spot diameter was estimated to be 2 $\mu m^2$. The scattered light was dispersed by a grating of 1800 L $mm^{-1}$, and a thermoelectrically cooled charged coupled device (CCD) detector recorded the signal.

The Raman acquisition parameters (laser power, exposure time, and number of scans) were adapted for each sample to prevent saturation of the CCD detector. The laser power was limited to typically 300 $\mu$W during the measurements to avoid damage to the sample surfaces.

### 2.3.3 | Characterization of Surface Oxidation by Infrared Spectroscopy

Fourier transform infrared (FTIR) spectroscopy was performed with an INVENIO Bruker FTIR spectrometer to estimate surface oxidation during treatments. Attenuated total reflectance (ATR) was carried out with a diamond crystal. The infrared spectrum was acquired within the 4000–400 $cm^{-1}$ spectral range using a deuterated triglycine sulfate (DTGS) detector. The infrared acquisition parameters were 4 $cm^{-1}$ for the resolution and 100 scans for accumulation.

## 3 | Results

## 3.1 | Effect of UV Irradiation on Pigment-Caused Luminescence

In the first section, we focus on the luminescence generated by the pigments. Commonly incorporated in plastics, pigments represent a serious limitation for Raman spectroscopy in the study of plastic pollution. To qualify the effect of UV treatment, a physicochemical characterization of the samples was performed.

Figure 1 displays the optical images and the Raman spectra of the green and blue untreated caps. Figure 1a highlights the luminescence phenomenon present between 700 $cm^{-1}$ and 1800 $cm^{-1}$ associated with an absence of any detectable Raman signal. For both caps, a gap between the maximum intensity was noted ($I_{max,green} = 34133\ cps$ and $I_{max,green} = 20200\ cps$). It is explained by the difference in pigments responsible to the luminescence. Also, a greater intra-sample variability for the green cap ($\sigma_{green} = 13940\ cps$ and $\sigma_{blue} = 4243\ cps$) caused by the heterogeneity of the photoluminescence signal on the surface is observed. Chemical identification is impossible with such spectra. Figure 1b reveals the presence of a low signal Raman between 2700 $cm^{-1}$ and 3200 $cm^{-1}$. Match scores of 85 ± 6.5% and 95 ± 2.0%, based on two Raman bands, were obtained for the green and blue polyethylene caps respectively with the Wire software (Renishaw company) (Figure 1b). To obtain specific data on additives, it is necessary to have Raman signatures from the so-called fingerprint region in the range 700–1800 $cm^{-1}$. Identification of the polymer was confirmed by infrared spectroscopy (Figure S1, Table S1 [Supporting Information]). The next sections present the effects of wavelength on luminescence caused by pigments. Several factors such as irradiance, humidity, and wavelength have been studied.

### 3.1.1 | Impact of Irradiance on the Luminescence

Figure 2 shows the decrease of photoluminescence after the treatment UV-076 and UV-083 for (a,b) green and (c,d) blue caps. Raman spectra of green caps (Figure 2a,b) exhibit an obvious decrease of luminescence and displayed new vibrational modes for both treatments. Raman signals of polyethylene (triangles) and green pigments (black stars) are now clearly visible. Contrary to infrared spectroscopy, the signature of these pigments was observed by Raman spectroscopy. The decrease of maximum intensity when treatment time increase confirmed the efficiency of the treatments for the green caps. The same

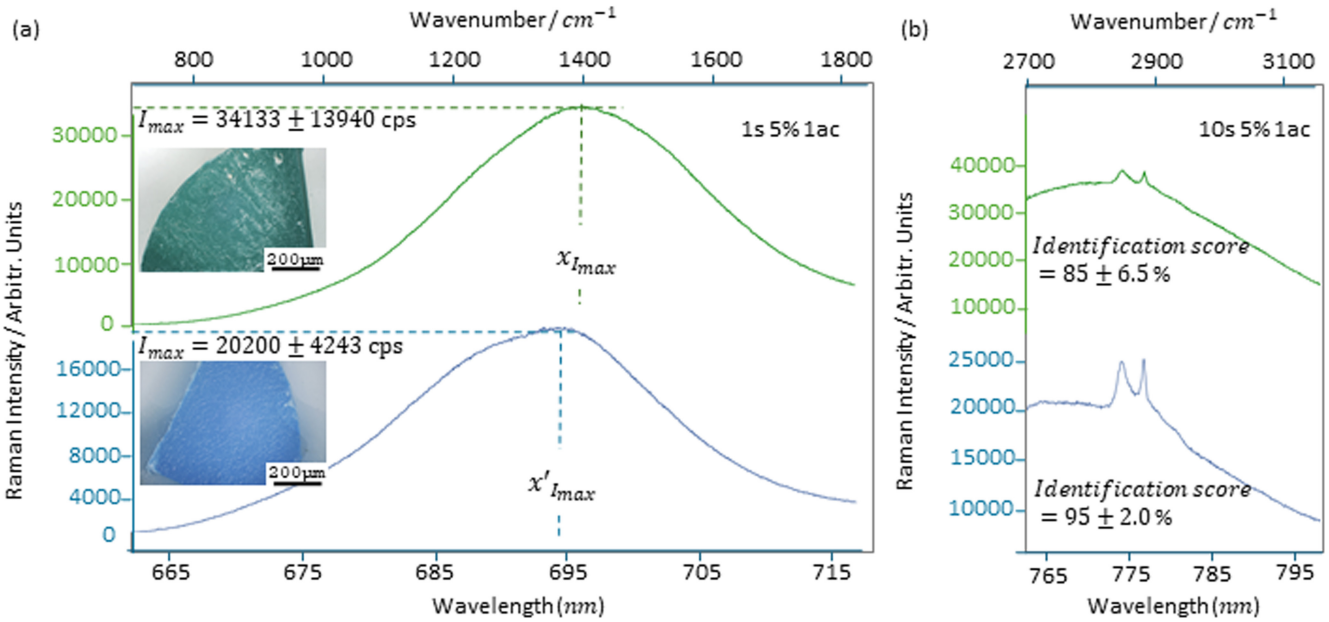


**FIGURE 1** | Optical microscopy and average Raman spectra between (a) 700–1800 $cm^{-1}$ and (b) 2700–3200 $cm^{-1}$ of unaged polyethylene from green and blue bottle caps.

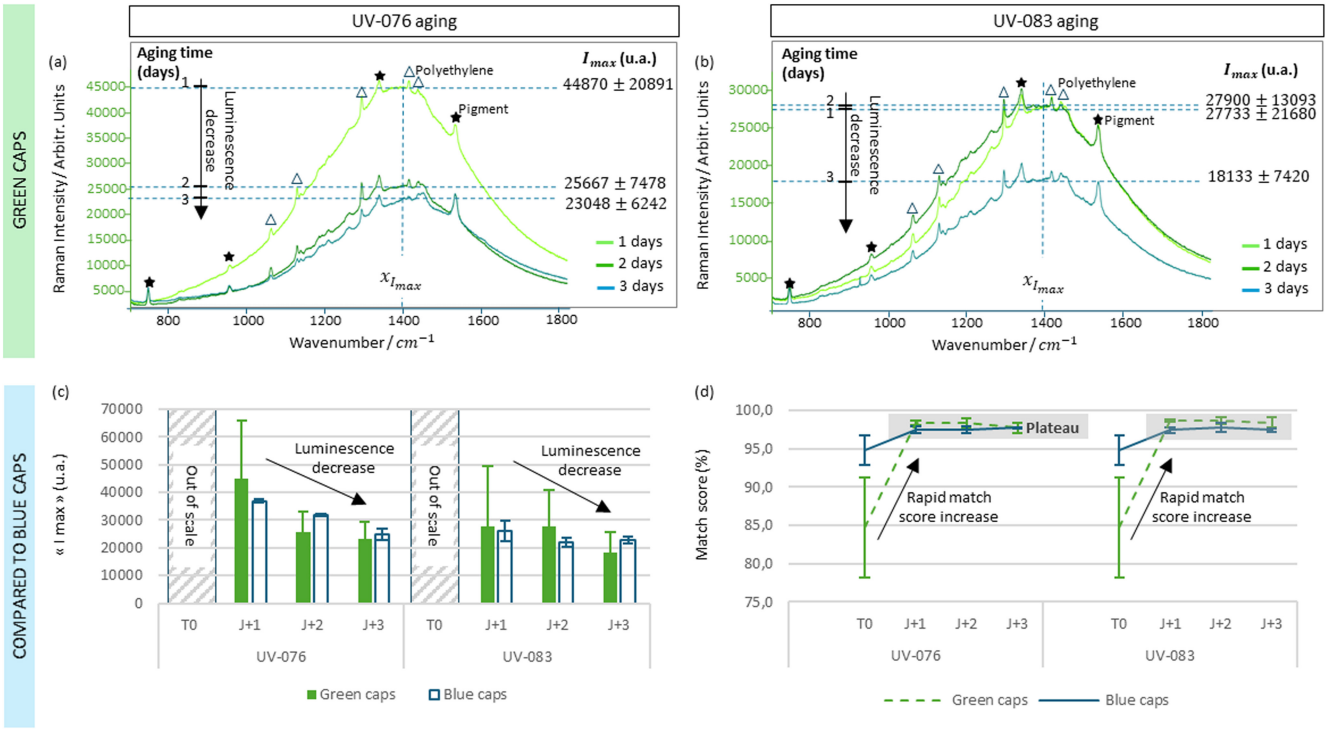


**FIGURE 2** | Average Raman spectra between 700 $cm^{-1}$ and 1800 $cm^{-1}$ of green caps aged 1, 2, and 3 days in (a) UV-076 and (b) UV-083 conditions. Comparison of results with blue caps aged under the same conditions (c,d).

trend was observed for the blue caps (Figure 2c). It was noted that the decrease in luminescence is proportional to the duration of treatment. In the short term (1 day), a decrease in maximum intensity was observed for the both cap colors (Figure 2c). After 2 and 3 days, a new decrease in maximum intensity and a reduction in standard deviation were observed. Overall, the decrease in standard deviation was explained by a homogenization of UV exposure across the entire surface. Between the two processes, the UV-083 treatment was more effective in reducing the maximum intensity, even if the two spectra overlap over the long term (Figure 2c). Regarding the identification score, an increase was observed on the first day of UV-076 and UV-083 treatment followed by a plateau after 2 and 3 days (Figure 2d). For example, the green cap treated 1 day under UV-076 and UV-083 showed a respective match score of $\%_{corr,J1(UV-076)} = 98 \pm 0.2$ and $\%_{corr,J1(UV-083)} = 99 \pm 0.1$. In fact, 1 day of exposure was sufficient to increase the correlation score, but longer treatment makes Raman modes more visible (Figure 2a,b).

**TABLE 2** | Evolution of infrared functional groups after 1, 2, 3 days of UV-076 and UV-083 treatments for green and blue caps [52].

| | | | Functional IR peak position ($cm^{-1}$) | | | | |
|---|---|---|---|---|---|---|---|
| **Time (days)** | | | **3600–3200** | **2300** | **1715** | **1655** | **1100–1000** |
| **Groups** | | | **Hydroxyl** | **Carbonyl** | **Carbonyl** | **Vinyl** | **Unknown** |
| Green caps | UV–076 | 1 | = | A | + | + | = |
| | | 2 | + | A | + | + | + |
| | | 3 | − | A | − | − | − |
| | UV–083 | 1 | + | = | + | + | + |
| | | 2 | − | = | − | − | − |
| | | 3 | = | + | = | = | = |
| Blue caps | UV–076 | 1 | + | A | + | + | = |
| | | 2 | = | A | + | + | = |
| | | 3 | = | A | − | − | = |
| | UV–083 | 1 | + | = | + | + | = |
| | | 2 | = | = | − | = | = |
| | | 3 | − | = | − | − | = |

*Note:* +, increase;−, decrease; =, invariant; A, absent.

The observation that the photoluminescence associated to pigments does not completely vanish under UV treatment can be explained by the lower penetration depth of UV radiation into the polymer compared to the excitation wavelength of the laser. The laser probes into a depth that exceeds that of efficient photobleaching and therefore sees incomplete photobleaching.

To complete this initial observation, infrared spectroscopy (Table 2, Figure S2 [Supporting Information]) and optical microscopy were performed (Figure S3 [Supporting Information]). Infrared spectra of green and blue UV-076 and UV-083 aged caps indicate the formation of new functional groups (carbonyl, hydroxyl, and vinyl). Their erratic evolutions are summarized in the Table 2. The presence of oxygenated functional groups highlights the photo-oxidation of the polymer surface during the treatments. Optical microscopy reveals no physical modifications on the sample surface during both treatments (no crack, no fissure) with a conservation of the initial roughness (Figure S3 [Supporting Information]). Additionally, no visual discoloration was observed.

In summary, we have demonstrated for the green and blue caps that the UV-076 and UV-083 treatments have a positive effect on the reduction of the luminescence (Figure 2c). A slight chemical modification on the surface of samples was identified by infrared spectroscopy (Table 2). An accelerated decrease in luminescence over a short exposure time (1 day) was shown as irradiance was increased. For longer periods (3 days), UV-076 and UV-083 converged towards identical maxima intensity and match scores, indicating incomplete photobleaching within the confocal volume. The decrease of luminescence associated with the apparition of Raman modes suggests that our protocol is efficient for different pigments. For pristine samples, the rate of decrease in luminescence depends on the pigment (Figure 2c).

### 3.1.2 | Humidity Influence

Figure 3 shows the evolution of luminescence phenomenon and match score during the UV-night and humid UV treatments for both caps. The green and blue aged caps exhibit a reduction of maximum intensity for both treatments (Figure 3a), accompanied by the apparition of Raman signals between 700 $cm^{-1}$ and 1800 $cm^{-1}$ (Figure S4 [Supporting Information]). The photobleaching is enhanced compared to the previous experiments without water.

The process "UV-night" and "humid UV" provide additional Raman bands between 700 $cm^{-1}$ and 1800 $cm^{-1}$ that were not observed upon continuous UV treatment and that we attribute to the unintentional increase of temperature from 45 to 60°C (Figure S4 [Supporting Information]). Depending on pigments, a different trend in the effectiveness of short-term luminescence reduction was observed (Figure 3a). In the specific case of green caps, humid UV treatment showed a rapid decrease in luminescence after only 1 day of exposure. Also, a larger number of Raman peaks were observed following the addition of humidity in the process (Figure S4 [Supporting Information]). This difference in Raman signature is attributed to the influence of the humid phase on the pigment at the origin of luminescence, most likely due to the synergistic effect between photolysis and hydrolysis. Finally, Figure 3b highlights a superposition of match scores for both samples treated (green and blue caps) over the same period in UV-night and humid UV conditions. After 1 day of exposure, the match score exceeded 97% for both samples and treatments.

Infrared spectra of green and blue aged caps confirmed the formation of hydroxyl (3400–3200 $cm^{-1}$), carbonyl (1800–1680 $cm^{-1}$), and vinyl (1640 $cm^{-1}$) groups during the UV-night and humid UV process (Figure S5 [Supporting Information]).

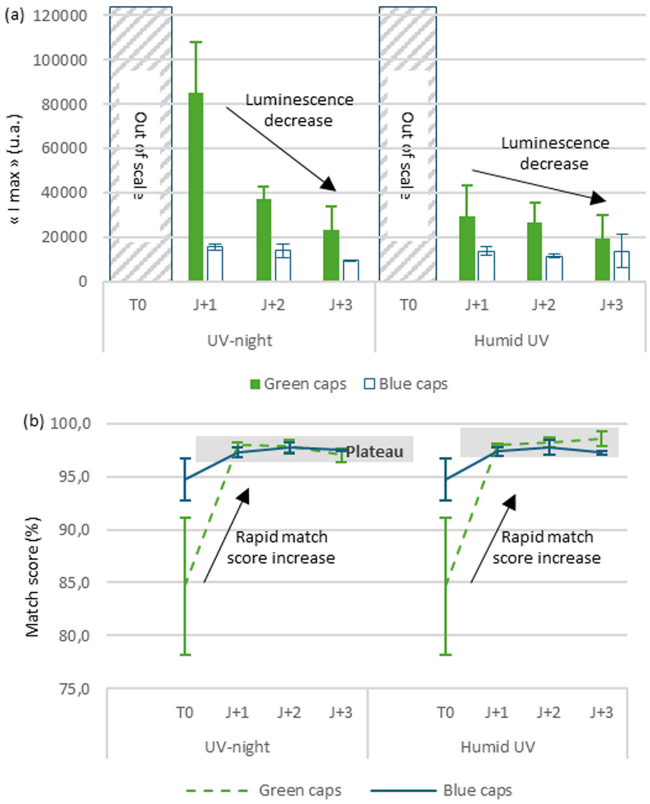


**FIGURE 3** | Estimated (a) decrease of the luminescence and (b) increase of the identification score during the UV-night and humid UV illumination time (1, 2, and 3 days) for the green and blue caps.

An increase in absorbance of the infrared modes was noted when the samples were subjected to UV-night treatment compared to UV-076 or UV-083 process. This elevation is attributed to an increase in surface oxidation resulting from a rise in temperature during UV irradiation. In fact, UV-076 and UV-083 were performed at 45 °C, whereas the UV-night and humid UV were realized at 60 °C for the UV exposition. Moreover, infrared spectra of humid UV aged caps highlight the formation of an additional band at 2300 $cm^{-1}$ attributed to carbonyl groups compared to UV-night treatment (Figure S5 [Supporting Information]). The random evolution of functional groups and impurity absorbance demonstrated the complexity of the mechanisms leading to the decrease in luminescence (Table S2, Table S3 [Supporting Information]). Optical images acquired with Leica microscope did not show any microscopical surface degradation for green and blue caps subjected to UV-night and humid UV treatments (Figure S6 [Supporting Information]).

In summary, UV-night and humid UV treatments have been performed on green and blue caps to reduce luminescence. Both procedures yield the same saturation value for the match score (Figure 3). Between UV-night and humid UV treatments, additional Raman signals were highlighted with the humid cycle (Figure S4 [Supporting Information]). In comparison to UV-076 and UV-083 treatments, new bands in Raman spectra were observed (Figure S4, red star [Supporting Information]) and attributed to an increase in temperature (from 45 to 60 °C) inside the chamber during the UV irradiation. An elevation of the surface oxidation was evidenced by an increase of absorption of the oxygen and vinyl groups on infrared spectra after UV-night and humid UV treatments (Figure S5 [Supporting Information]). Second, the impact of the humid cycle was confirmed by the presence of an infrared band at 2300 $cm^{-1}$, not present after UV-night treatment (Figure S5 [Supporting Information]). This result suggests an activation of supplementary reaction(s) in the presence of water, certainly attributable to the photogeneration of radicals. Finally, no physical modification of the surface structure was observed (Figure S6 [Supporting Information]).

### 3.1.3 | Wavelength Effect

Figure 4 displays the evolution of the luminescence between 700 $cm^{-1}$ and 1800 $cm^{-1}$ when green and blue caps were exposed to UV radiation and spontaneously formed ozone inside the chamber ($\lambda = 254$ nm and 185 nm) treatment for a few minutes to a few hours. A gradual decrease of the maximum intensity was noted (Figure 4a). Before treatment, no Raman signature was observed but the reduction of photoluminescence in combination with an increase of Raman acquisition parameters (time acquisition, laser power) provided access to Raman signal after 300 min of exposure. An example of a Raman spectrum recorded on the green cap treated 300 min is presented in Figure 4b. After UV ozone treatment, vibrational modes of polyethylene (triangles) and pigments (black stars) were revealed. Raman signatures of pigments was observed while they remained undetectable in FTIR spectra. Compared to other treatments, a higher reduction in luminescence was obtained after a much shorter UV illumination duration. This result demonstrates the enhanced effectiveness of UV-$O_3$ treatment in reducing luminescence.

Figure 4c superimposes the evolution of match score and acquisition time for both cap colors. Before UV ozone treatment, no consistent identification was obtained. For the green cap, it took just 15 min to identify the correct polymer (polyethylene) from the database. The reduction in luminescence during the process allowed for an increase in acquisition time without detector saturation, which resulted in an increased match score. After 60 min, the identification score exceeded 90%, reaching 97% after 240 min of treatment. Concerning blue caps, no clear identification was possible before 60 min of treatment. The gradual decrease in luminescence allowed for the identification of polyethylene after 60 min of treatment. At 240 min and 300 min, the lower luminescence intensity allowed again for an extended acquisition time, resulting in match scores of 98% and 99%, respectively. For both samples, UV ozone treatment revealed a high efficiency.

Table 3 displays the qualitative evolution of new infrared functional groups and impurities during the UV ozone treatment of the green and blue caps. Contrary to previous treatments, infrared spectra show the absence of a band around 2300 $cm^{-1}$ (for both caps) and bands between 3600 and 3200 $cm^{-1}$ (green caps). This difference between caps demonstrates the impact of additives on the stabilisation of samples under UV exposure. The absorbance fluctuation on the remaining functional bands again shows the complexity of the mechanisms involved in surface oxidation (and reduced luminescence) (Table 3), which goes beyond the scope of this study. Eventually, optical microscopy

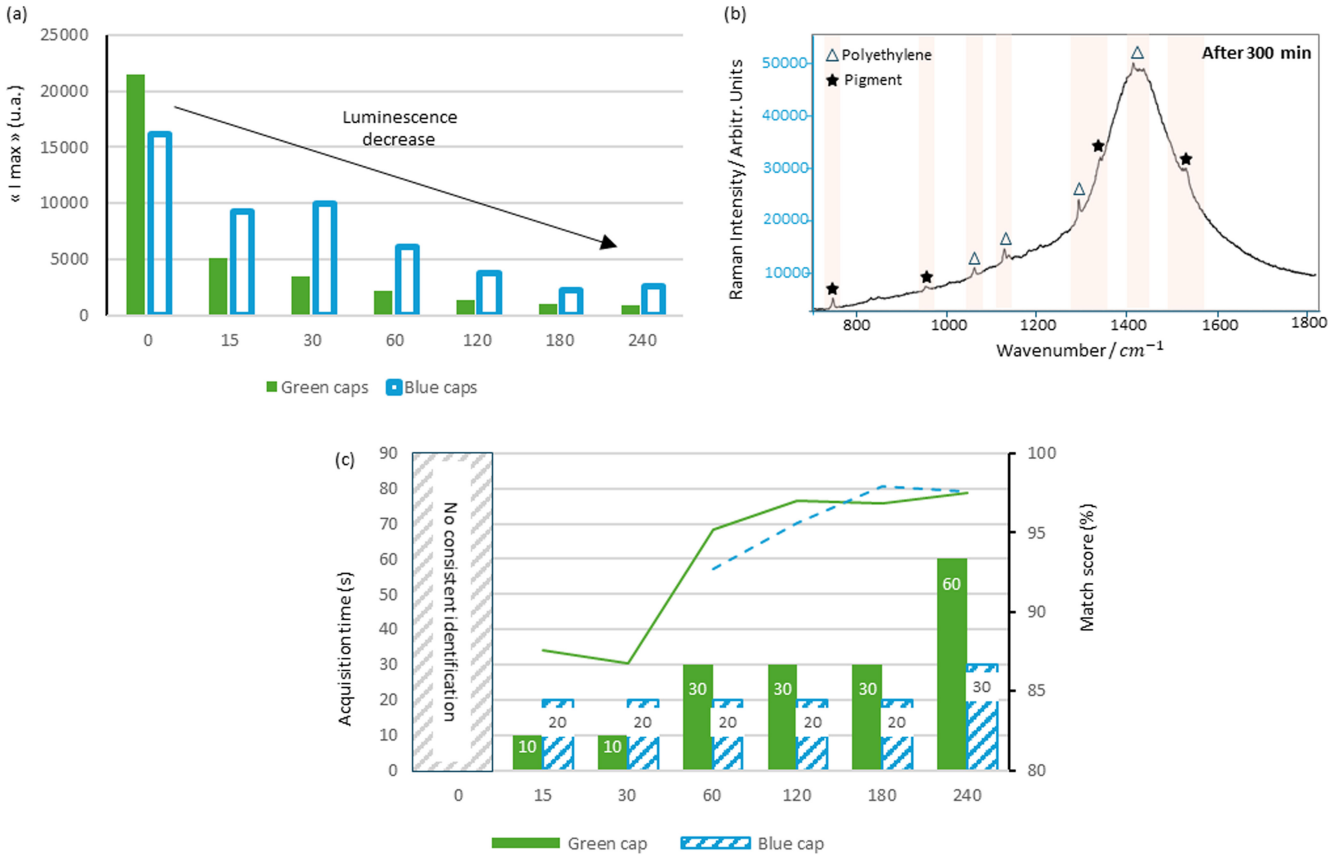


**FIGURE 4** | (a) Estimated decrease of the luminescence between 700 $cm^{-1}$ and 1800 $cm^{-1}$ of green and blue caps exposed to UV ozone treatment during 15, 30, 60, 120, 180, and 240 min. (b) Raman spectra of blue cap aged 300 min. The triangles and the black stars are respectively attributed to polyethylene bands and additives bands. The beige zone highlights the presence of one or more Raman signals. (c) Acquisition time (sticks) and match score (curves) of blue and green caps exposed to UV ozone treatment during 15, 30, 60, 120, 180, and 240 min.

**TABLE 3** | Infrared vibrational mode evolution of functional groups during the UV ozone treatment for green and blue caps [53].

| | | Functional IR peak position ($cm^{-1}$) | | | | | |
|---|---|---|---|---|---|---|---|
| **Time (days)** | | **3600–3200** | **2300** | **1715** | **1655** | **1420** | **1100–1000** |
| **Groups** | | **Hydroxyl** | **Carbonyl** | **Carbonyl** | **Vinyl** | **Aldehyde** | **Unknown** |
| Green caps UV ozone | 60 | A | A | + | + | + | = |
| | 120 | A | A | − | − | + | = |
| | 180 | A | A | − | = | + | = |
| | 240 | A | A | + | = | − | = |
| | 300 | A | A | + | = | − | = |
| Blue caps UV ozone | 60 | = | A | + | + | + | = |
| | 120 | + | A | − | + | − | = |
| | 180 | − | A | − | = | − | = |
| | 240 | = | A | = | - — | − | = |
| | 300 | = | A | + | + | + | = |

*Note:* +, increase; −, decrease; =, invariant; A, absent.

of green and blue aged caps again did not reveal any physical degradation (cracks, fissures) during the UV ozone process (Figure S7 [Supporting Information]). Once again, no discoloration was perceivable at the macroscopic scale.

To resume, the UV ozone treatment on green and blue caps has demonstrated a higher decrease in luminescence than the previous methods (UV-076, UV-083, UV-night, and humid UV) (Figure 4). Non-conjugated polymers require wavelengths

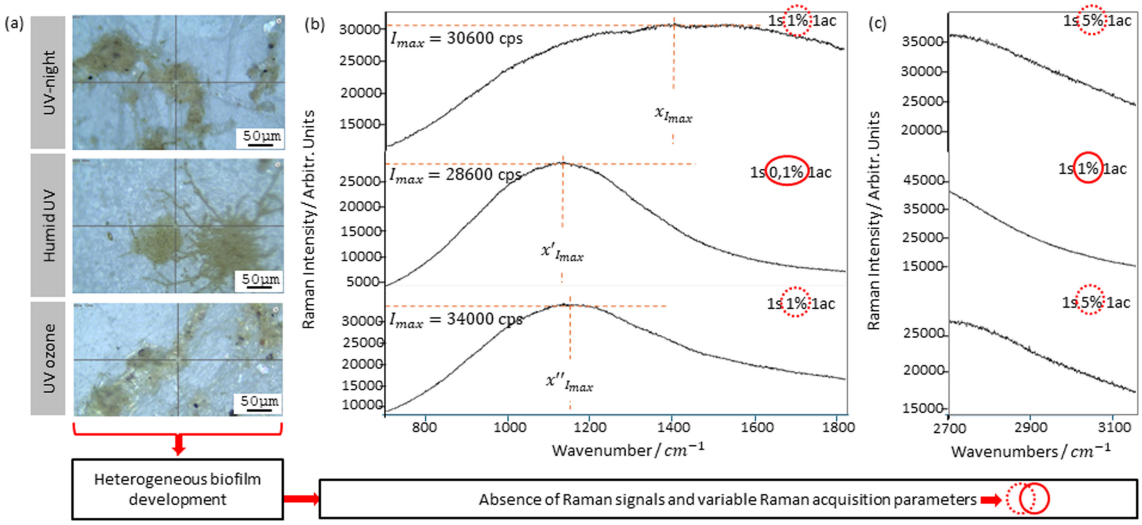


**FIGURE 5** | (a) Optical images and Raman spectra in the spectral range (b) 700–1800 $cm^{-1}$ and (c) 2700–3200 $cm^{-1}$ of unaged white caps recovered by biofilm.

below 200 nm for the fundamental absorption of the polymer backbone (in contrast to conjugated polymer systems that might absorb even in the visible range). For this reason, we consider that most of the photochemistry that we observe originates from the sub-gap absorption via e.g., defects and interaction with mainly undocumented additives. The infrared spectra displayed a decrease in the number of new functional groups during the treatment (Table 3), which suggests that different or additional degradation mechanisms are at play in the presence of ozone. As Bourgogne et al. [53] showed, the change in wavelength has an influence on the photodegradation mechanisms involved and, consequently, on the effectiveness of the treatments in reducing the luminescence background. The efficacy of the treatment depends on the nature of the additive and at this point, the UV-$O_3$ treatment is the most efficient method.

## 3.2 | Effect of Continuous UV Irradiation on Luminescence Caused by Biofilm

In this second section, the impact of continuous UV irradiation on the luminescence caused by the colonization of microorganisms on the surface of samples was studied. The existence of bioluminescence, encountered when measuring samples collected after a prolonged stay in sea, is a major impediment for the study of plastic pollution. At present, mainly chemical treatments are used to remove the biofilm layer [54].

A qualitative comparison of results between treatments was conducted taking into account the heterogeneous development of biofilms on the microscopic scale. As can be seen in Figure 5, the surface colonized was a white cap, which showed no luminescence overlapping with the Raman spectra before immersion. An additional luminescence was induced by the presence of the biofilm alone.

Figure 5 displays the initial state of each biofilm selected for UV-night, humid UV, and UV ozone treatments. Figure 5a shows the surface morphology before treatment and highlights the heterogeneous microscopic development of biofilms. Figure 5b,c illustrates the emission spectra of biofilms between 700–1800 $cm^{-1}$ and 2700–3200 $cm^{-1}$. For all spectra, an intense background of bioluminescence was observed and superseded the Raman signal to the extent of preventing the chemical identification of the substrate (Figure 5b,c). For the humid UV treatment, luminescence was still high and required a lower laser power (0.1%) to avoid detector saturation caused by this luminescence (Figure 5a,b). The difference in Raman acquisition parameters confirmed the heterogeneous microscopic biofilm development on the sample surface.

### 3.2.1 | Impact of Continuous UV Irradiation

Figure S8 (Supporting Information) illustrates the effect of UV-night treatment on the biofilm partially covering the white cap. The superposition of untreated and treated Raman spectra highlighted a decrease in peak intensity in the spectral range 700–1800 $cm^{-1}$ and 2700–3200 $cm^{-1}$ during the UV-night exposure. For the first 2 days, a rapid decrease is observed, with a reduction of 50%. At 3 days of exposure, a slight additional decrease was obtained, but still no Raman signal was observable in the two spectral ranges analyzed (Figure S8 [Supporting Information]). Here, the biofilm creates a barrier between the laser and the substrate, leading to the spectral signature of the polymer being masked by the photoluminescence of the biofilm. The thickness of the biofilm is a factor limiting the applicability of the treatment. In fact, the mechanisms involved in UV-night exposure of the biofilm generated a global diminution of the initial luminescence. Indeed, the peak intensity converged to a steady value over long times. Finally, the microscopy images in Figure S8 (Supporting Information) show no physical modification neither on the white cap surface nor on biofilm (no crack, no discoloration, etc.).

### 3.2.2 | Influence of Humidity

Figure 6 depicts Raman spectra and images recorded on a biofilm subjected to humid UV treatment during 1, 2, and 3 days.

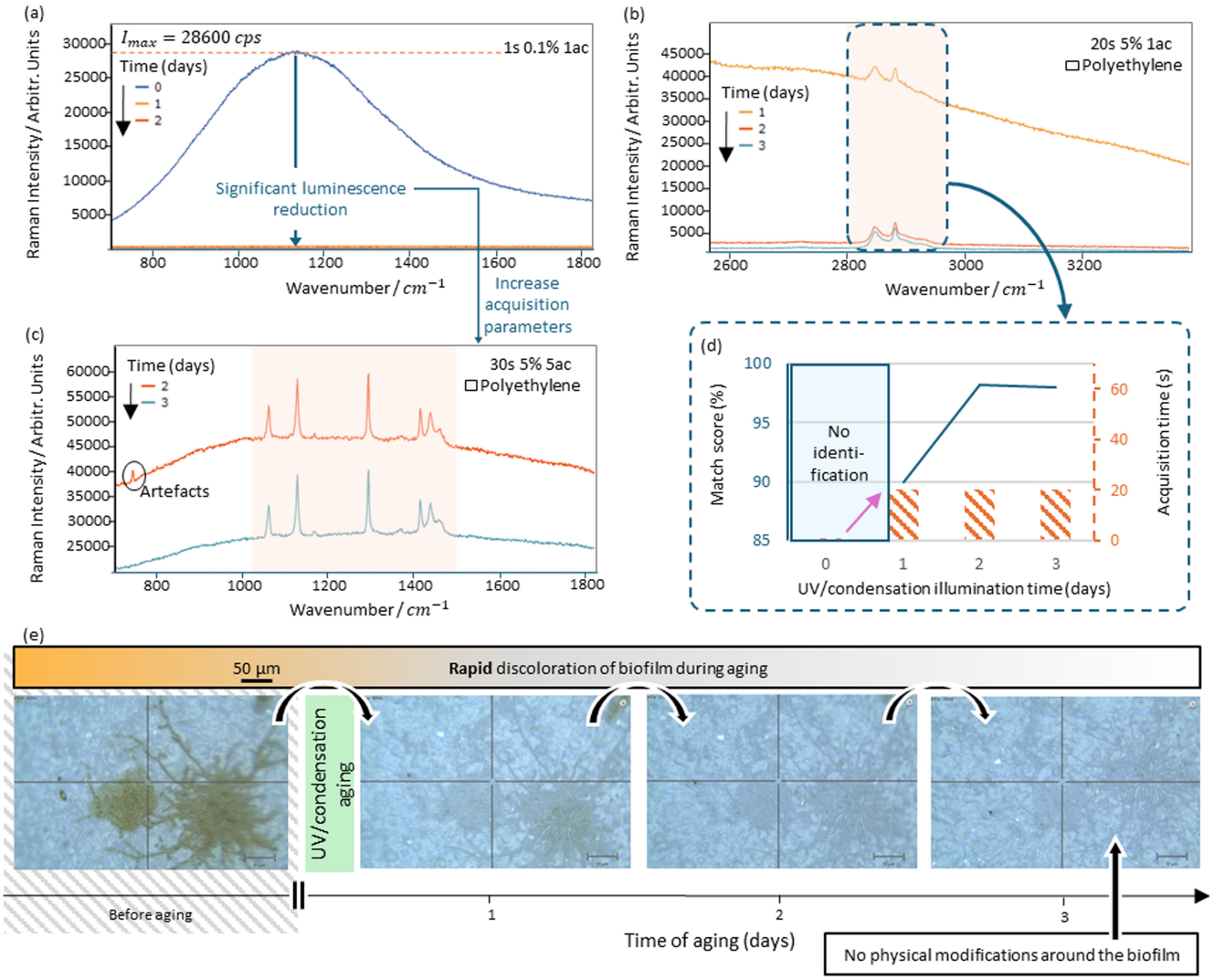


**FIGURE 6** | Raman spectra between (a) 700–1800 $cm^{-1}$ and (b) 2700–3200 $cm^{-1}$, with a focus on signals centered at 1300 $cm^{-1}$ of white recovered caps exposed to humid UV process. (d) Estimated match score between 2700 and 3200 $cm^{-1}$ and (e) Raman imaging associated.

The Raman spectra indicate a sharp drop in luminescence from day one (Figure 6a). In the spectral range 700–1800 $cm^{-1}$ and 2700–3200 $cm^{-1}$, an increase in the acquisition time and laser power resulted in detectable Raman signals (Figure 6b,c). The match score analysis in Figure 6d reveals reliable polymer identification after the first day of treatment. The decrease in luminescence visualized between days 2 and 3 resulted in a further increase of the match score ($\%_{corr,2j} = 98\%$) with stabilization for longer times ($\%_{corr,3j} = 98\%$) (Figure 6c,d). Under the microscope, a discoloration during process was noted indicating biofilm deterioration (Figure 6e) even though residues remain visible.

Compared to the previous UV-night treatment, several Raman bands are visible in Figure 6b,c even though the initial biofilm luminescence was higher (Figure 5). These results highlight the relevance of humidity for the reduction of the biofilm luminescence. In contrast to the previous case of UV exposure under dry conditions, a substantial biofilm degradation was observed (Figure 6e). We assume that several mechanisms, such as hydrolysis and photo-oxidation, are involved, almost certainly simultaneously. The complementarity of the mechanisms has led to a significant reduction in luminescence, with polymer identification exceeding 97%. The involvement of one or more additional mechanisms will be subject of further investigation to establish a link between the biofilm deterioration and the increase of Raman signals (Figure 6).

### 3.2.3 | Effect of the UV Wavelength on the Efficacy of Luminescence Suppression

Figure S9 (Supporting Information) presents Raman results when a biofilm is subjected to UV ozone treatment. Raman spectra between 700–1800 $cm^{-1}$ and 2700–3200 $cm^{-1}$ show a global decrease in luminescence during the treatment. At the end of the treatments, the luminescence converges towards a stable peak value, and yet, no Raman signals are detectable. Between 180 min and 300 min of UV-night exposure, an increase in the two spectral ranges of interest was observed. In terms of physical structure, a slight discoloration of biofilm was identified with no morphological modification of the substrate (Figure S9 [Supporting Information]). This treatment highlighted a positive and limited effect of the UV ozone process

with a progressive decrease in luminescence; however, it was insufficient to bring the statistical noise of the luminescence signal below the expected intensity of the Raman signals, resulting in the impossibility to identify the substrate by Raman spectroscopy. However, a decrease in luminescence was demonstrated when the substrate covered by biofilm was exposed to UV ozone treatment.

Tjandraatmadja et al. [55] have demonstrated the ability of certain biofilm components to absorb UV radiation in specific ranges. A biofilm can protect the substrate by attenuating UV penetration. For example, an exopolysaccharide matrix absorbs between 240 and 280 nm. Consequently, a change in wavelength influences the penetration of UV radiation and impacts the effectiveness of treatments [56].

## 4 | Conclusions

We demonstrated the efficiency of UV photobleaching pretreatment to reduce the luminescence background encountered in Raman spectroscopy of plastics. Five different treatments were performed to optimize the protocol and study the influence of various parameters (irradiance, humidity, wavelength, time). All of them can be easily reproduced without any costly and complex UV illumination system, which appears extremely promising in the field of plastic pollution where the presence of pigments and surface contaminants such as biofilm usually prevents identification though Raman spectroscopy. Our protocol proved its efficiency in reducing the luminescence background regardless of its origin, allowing a chemical identification in conditions where it was not possible with the pristine samples. Nevertheless, we would like to emphasize that the experimental parameters reported here are specific to our samples. The efficient use of the UV photobleaching requires optimization of the process (dry or humid, UVA or UVC irradiation, illumination time) and strongly depends on the history and nature of the plastic sample. In the case of luminescence caused by pigments, we observed that the UV wavelength was the key parameter, independently of the presence of humidity in the chamber. In opposition, when a biofilm was present on the surface, humidity was necessary to achieve chemical identification of the plastic. The influence of these multiple parameters highlights the complex photochemical reactions that occur during the UV photobleaching process even if the method proved effective. Understanding those mechanisms will require further dedicated studies.

### Author Contributions

**L. Dewyspelaere:** conceptualization, data curation, investigation and writing – original draft. **L. Belec:** conceptualization and writing – review and editing. **I. Martin:** conceptualization, investigation and writing – review and editing. **V. Lenoble:** resources and writing – review and editing. **A. Ruediger:** writing – review and editing. **A. Merlen:** conceptualization, funding acquisition, supervision and writing – review and editing.


### Acknowledgments

We would like to thank Annick Ortalo-Magne, Raphaëlle Barry-Martinet, and Jean-François Briand for their constructive comments and suggestions. We gratefully acknowledge Mélanie Wolfs for her insightful guidance and constant support regarding the aging chambers. Open access publication funding provided by COUPERIN CY26.

### Funding

The authors have nothing to report.


### Conflicts of Interest

The authors declare no conflicts of interest.

### Data Availability Statement

The data that support the findings of this study are available from the corresponding author upon reasonable request.

### References


1. D. Seo, D. Lim, J. Seo, and D. Shin, "Quantification of Auto-Photobleaching Effects During Raman Measurements for Microplastic Detection," *Sensors and Actuators B: Chemical* 423 (2025): 136702.

2. PlasticsEurope (2024).

3. R. Geyer, J. R. Jambeck, and K. L. Law, "Production, Use, and Fate of All Plastics Ever Made," *Science Advances* 3, no. 7 (2017): e1700782.

4. T. R. Walker and L. Fequet, "Current Trends of Unsustainable Plastic Production and Micro (Nano) Plastic Pollution," *TrAC Trends in Analytical Chemistry* 160 (2023): 116984.

5. J. L. Xu, K. V. Thomas, Z. Luo, and A. A. Gowen, "FTIR and Raman Imaging for Microplastics Analysis: State of the Art, Challenges and Prospects," *TrAC Trends in Analytical Chemistry* 119 (2019): 115629.

6. Y. Xiang, L. Jiang, Y. Zhou, et al., "Microplastics and Environmental Pollutants: Key Interaction and Toxicology in Aquatic and Soil Environments," *Journal of Hazardous Materials* 422 (2022): 126843.

7. J. G. B. Derraik, "The Pollution of the Marine Environment by Plastic Debris: A Review," *Marine Pollution Bulletin* 44 (2002): 842–852.

8. N. Rafa, B. Ahmed, F. Zohora, et al., "Microplastics as Carriers of Toxic Pollutants: Source, Transport, and Toxicological Effects," *Environmental Pollution* 2024, no. 343 (1987): 123190.

9. B. Xi, B. Wang, M. Chen, et al., "Environmental Behaviors and Degradation Methods of Microplastics in Different Environmental Media," *Chemosphere* 299 (2022): 134354.

10. S. Huppertsberg and T. P. Knepper, "Instrumental Analysis of Microplastics—Benefits and Challenges," *Analytical and Bioanalytical Chemistry* 410 (2018): 6343–6352.

11. S. L. Wright and F. J. Kelly, "Plastic and Human Health: A Micro Issue?," *Environmental Science & Technology* 51 (2017): 6634–6647.

12. A. Tirkey and L. S. Upadhyay, "Microplastics: An Overview on Separation, Identification and Characterization of Microplastics," *Marine Pollution Bulletin* 170 (2021): 112604.

13. P. G. Nayanathara Thathsarani Pilapitiya and A. S. Ratnayake, "The World of Plastic Waste: A Review," *Cleaner Materials* 11 (2024): 100220.

14. Z. Feng, L. Zheng, and J. Liu, "Classification of Household Microplastics Using a Multi-Model Approach Based on Raman Spectroscopy," *Chemosphere* 325 (2023): 138312.

15. E. Dümichen, P. Eisentraut, C. G. Bannick, A. K. Barthel, R. Senz, and U. Braun, "Fast Identification of Microplastics in Complex Environmental Samples by a Thermal Degradation Method," *Chemosphere* 174 (2017): 572–584.

16. A. Käppler, D. Fischer, S. Oberbeckmann, et al., "Analysis of Environmental Microplastics by Vibrational Microspectroscopy: FTIR,

Raman or Both?," *Analytical and Bioanalytical Chemistry* 408 (2016): 8377–8391.

17. A. M. Macdonald and P. Wyeth, "On the Use of Photobleaching to Reduce Fluorescence Background in Raman Spectroscopy to Improve the Reliability of Pigment Identification on Painted Textiles," *Journal of Raman Spectroscopy* 37 (2006): 830–835.

18. A. P. Kotula, S. V. Orski, K. C. Brignac, J. M. Lynch, and B. M. Heilala, "Time-Gated Raman Spectroscopy of Recovered Plastics," *Marine Pollution Bulletin* 181 (2022): 113894.

19. A. Azari, S. Ronsmans, J. A. J. Vanoirbeek, P. H. M. Hoet, and M. Ghosh, "Challenges in Raman Spectroscopy of (Micro)Plastics: The Interfering Role of Colourants," *Environmental Pollution* 2024, no. 363 (1987): 125250.

20. C. F. Araujo, M. M. Nolasco, A. M. P. Ribeiro, and P. J. Ribeiro-Claro, "Identification of Microplastics Using Raman Spectroscopy: Latest Developments and Future Prospects," *Water Research* 142 (2018): 426–440.

21. N. P. Ivleva, P. Kubryk, and R. Niessner, "Raman Microspectroscopy, Surface-Enhanced Raman Scattering Microspectroscopy, and Stable-Isotope Raman Microspectroscopy for Biofilm Characterization," *Analytical and Bioanalytical Chemistry* 409 (2017): 4353–4375.

22. S. Primpke, S. H. Christiansen, W. Cowger, et al., "Critical Assessment of Analytical Methods for the Harmonized and Cost-Efficient Analysis of Microplastics," *Applied Spectroscopy* 74 (2020): 1012–1047.

23. V. Nava, M. L. Frezzotti, and B. Leoni, "Raman Spectroscopy for the Analysis of Microplastics in Aquatic Systems," *Applied Spectroscopy* 75 (2021): 1341–1357.

24. J. Zięba-Palus and A. Michalska, "Photobleaching as a Useful Technique in Reducing of Fluorescence in Raman Spectra of Blue Automobile Paint Samples," *Vibrational Spectroscopy* 74 (2014): 6–12.

25. C. Coupry, "Application of Raman Microspectrometry to arts objects," *Analusis* 28 (2000): 39–45.

26. G. Renner, A. Nellessen, A. Schwiers, M. Wenzel, T. C. Schmidt, and J. Schram, "Data Preprocessing & Evaluation Used in the Microplastics Identification Process: A Critical Review & Practical Guide," *TrAC Trends in Analytical Chemistry* 111 (2019): 229–238.

27. K. Martin and H. Bryan, "Time-Gated Raman Spectroscopy - A Review," *Measurement Science and Technology* 32 (2020): 012002.

28. R. T. Vulchi, V. Morgunov, R. Junjuri, and T. Bocklitz, "Artifacts and Anomalies in Raman Spectroscopy: A Review on Origins and Correction Procedures," *Molecules (Basel, Switzerland)* 29 (2024): 4748.

29. K. Buckley and A. G. Ryder, "Applications of Raman Spectroscopy in Biopharmaceutical Manufacturing: A Short Review," *Applied Spectroscopy* 71 (2017): 1085–1116.

30. R. Lenz, K. Enders, C. A. Stedmon, D. M. A. Mackenzie, and T. G. Nielsen, "A Critical Assessment of Visual Identification of Marine Microplastic Using Raman Spectroscopy for Analysis Improvement," *Marine Pollution Bulletin* 100 (2015): 82–91.

31. A. H. Hamidian, E. J. Ozumchelouei, F. Feizi, C. Wu, Y. Zhang, and M. Yang, "A Review on the Characteristics of Microplastics in Wastewater Treatment Plants: A Source for Toxic Chemicals," *Journal of Cleaner Production* 295 (2021): 126480.

32. A. M. Elert, R. Becker, E. Duemichen, et al., "Comparison of Different Methods for MP Detection: What Can We Learn From Them, and Why Asking the Right Question Before Measurements Matters?," *Environmental Pollution* 2017, no. 231 (1987): 1256–1264.

33. P. M. Anger, E. von der Esch, T. Baumann, M. Elsner, R. Niessner, and N. P. Ivleva, "Raman Microspectroscopy as a Tool for Microplastic Particle Analysis," *TrAC Trends in Analytical Chemistry* 109 (2018): 214–226.

34. S. Ruiz-Moreno, A. López-Gil, A. Gabaldón, and C. Sandalinas, "Raman Spectroscopy and UV Pulsed Laser: An Excellent Symbiosis?," *Journal of Raman Spectroscopy* 35 (2004): 640–645.

35. Y. Liu, J. Hu, L. Lin, et al., "Overcoming the Fluorescent Interference During Raman Spectroscopy Detection of Microplastics," *Science of the Total Environment* 897 (2023): 165333.

36. D. Tuschel, "Selecting an Excitation Wavelength for Raman Spectroscopy," *Spectroscopy* 31 (2016): 14–23.

37. F. Schulte, K.-W. Brzezinka, K. Lutzenberger, H. Stege, and U. Panne, "Raman Spectroscopy of Synthetic Organic Pigments Used in 20th Century Works of Art," *Journal of Raman Spectroscopy* 39 (2008): 1455–1463.

38. M. G. J. Löder and G. Gerdts, "Methodology Used for the Detection and Identification of Microplastics - A Critical Appraisal," *Marine Anthropogenic Litter*, eds. M. Bergmann, L. Gutow, and M. Klages (Springer International Publishing, 2015), 201.

39. K. P. J. Williams and D. L. Gerrard, "The Use of 752.5 and 799.3 nm Laser Excitation in Raman Spectroscopy," *Optics and Laser Technology* 17 (1985): 245–248.

40. K. Golcuk, G. S. Mandair, A. F. Callender, N. Sahar, D. H. Kohn, and M. D. Morris, "Is Photobleaching Necessary for Raman Imaging of Bone Tissue Using a Green Laser?," *Biochimica et Biophysica Acta (BBA) - Biomembranes* 1758 (2006): 868–873.

41. F. Madonini and F. Villa, "Single Photon Avalanche Diode Arrays for Time-Resolved Raman Spectroscopy," *Sensors (Basel, Switzerland)* 21 (2021): 4287.

42. E. Vilella and A. Diéguez, "A Gated Single-Photon Avalanche Diode Array Fabricated in a Conventional CMOS Process for Triggered Systems," *Sensors and Actuators, A: Physical* 186 (2012): 163–168.

43. T. Rojalin, L. Kurki, T. Laaksonen, et al., "Fluorescence-Suppressed Time-Resolved Raman Spectroscopy of Pharmaceuticals Using Complementary Metal-Oxide Semiconductor (CMOS) Single-Photon Avalanche Diode (SPAD) Detector," *Analytical and Bioanalytical Chemistry* 408 (2016): 761–774.

44. D. Wei, S. Chen, and Q. Liu, "Review of Fluorescence Suppression Techniques in Raman Spectroscopy," *Applied Spectroscopy Reviews* 50 (2015): 387–406.

45. R. P. Van Duyne, D. L. Jeanmaire, and D. F. Shriver, "Mode-Locked Laser Raman Spectroscopy. New Technique for the Rejection of Interfering Background Luminescence Signals," *Analytical Chemistry (Washington)* 46 (1974): 213–222.

46. J. V. Gulmine, P. R. Janissek, H. M. Heise, and L. Akcelrud, "Degradation Profile of Polyethylene After Artificial Accelerated Weathering," *Polymer Degradation and Stability* 79 (2003): 385–397.

47. Libraries SJ.

48. R. Beer and R. H. Norton, "Analysis of Spectra Using Correlation Functions," *Applied Optics* 27 (1988): 1255–1261.

49. F. Adar, "A Simple Introduction to Raman Spectral Identification of Organic Materials," *Spectroscopy (Ottawa)* 36 (2021).

50. J. F. Kauffman, J. D. Rodriguez, and L. F. Buhse, "Spectral Preprocessing for Raman Searches," *American Pharmaceutical Review* 14 (2011): 34–40.

51. Spectragryph.

52. S. Phan, J. L. Padilla-Gamiño, and C. K. Luscombe, "The Effect of Weathering Environments on Microplastic Chemical Identification With Raman and IR Spectroscopy: Part I. Polyethylene and Polypropylene," *Polymer Testing* 116 (2022): 107752.

53. D. Bourgogne, S. Therias, and J.-L. Gardette, "Wavelength Effect on Polymer Photooxidation Under LED Weathering Conditions," *Polymer Degradation and Stability* 202 (2022): 110021.

54. V. Lenoble, A.-M. Cindrić, J.-F. Briand, et al., "Bioaccumulation of Trace Metals in the Plastisphere: Awareness of Environmental Risk From a European Perspective," *Environmental Pollution* 2024, no. 348 (1987): 123808.

55. G. F. Tjandraatmadja, L. S. Burn, and M. C. Jollands, "Evaluation of Commercial Polycarbonate Optical Properties After QUV-A Radiation—the Role of Humidity in Photodegradation," *Polymer Degradation and Stability* 78 (2002): 435–448.

56. I. Goßmann, H. Mitsutake, J. Degenhardt, M. E. Simonsen, and F. Liu, "Biofilms on Plastics Slow Photo-Oxidation while Promoting Surface Degradation," *Environmental Science & Technology* 59 (2025): 22866–22873.

## Supporting Information

Additional supporting information can be found online in the Supporting Information section. **Figure S1:** Infrared spectra of the (a) green and (b) blue untreated bottle caps. Beige and purple framed bands correspond to polyethylene and impurities. **Figure S2:** Infrared spectra of green bottle caps treated with (a) UV-076 and (b) UV-083. Beige, purple, and blue framed bands correspond to polyethylene, impurities, and functional groups. **Figure S3:** Raman imaging of (a) green and (b) blue caps treated with UV-076 and UV-083 during 1, 2, and 3 days. **Figure S4:** Raman spectra between 700 and 1800 cm−1 of (a,b) green and (c,d) blue caps treated 1, 2, and 3 days in (a,c) UV-night and (b,d) humid UV conditions. Triangles, entire black stars, and red stars correspond respectively to the attribution polyethylene, additives, and additional bands. **Figure S5:** Infrared spectra of (a) green and (b) blue caps treated 1, 2, and 3 days in (a) UV-night or (b) humid UV conditions. Beige, purple, and blue framed bands correspond to polyethylene, impurities, and functional groups. **Figure S6:** Microscopy image of (a) green and (b) blue caps treated with dry and humid UV during 1, 2, and 3 days. **Figure S7:** Microscopy image of (a) green and (b) blue caps treated with UV ozone during 1, 2, and 3 days. **Figure S8:** Raman spectra around (a) 1300 cm−1 and (b) 3000 cm−1. (c) Microscopy image of white recovered caps exposed to UV-night treatment. **Figure S9:** Raman spectra around (a) 1300 cm−1 and (b) 3000 cm−1 of white recovered caps exposed to UV ozone process. (e) Microscopy image of the region of interest. **Table S1:** With infrared vibrational mode identification for polyethylene. **Table S2:** With infrared vibrational mode evolution of functional groups during the UV-night and humid UV treatments of green caps. **Table S3:** With infrared vibrational mode evolution of functional groups during the UV-night and humid UV treatments of blue caps.